Available online at www.sciencedirect.com
ScienceDirect
Journal of Photochemistry and Photobiology A: Chemistry 185 (2007) 94–100
Journal of Photochemistry and Photobiology A:Chemistry
www.elsevier.com/locate/jphotochem

Excited-state energy transfers in single-walled carbon nanotubes functionalized with tethered pyrenes

Huaping Li [a], Muhammet Erkan Kose [a], Liangwei Qu [a], Yi Lin [a], Robert B. Martin [a], Bing Zhou [a], Barbara A. Harruff [a], Lawrence F. Allard [b], Ya-Ping Sun [a,*]

[a] *Department of Chemistry and Laboratory for Emerging Materials and Technology, Clemson University, Clemson, SC 29634-0973, USA*
[b] *High Temperature Materials Laboratory, Oak Ridge National Laboratory, Oak Ridge, TN 37831, USA*

Received 7 March 2006; received in revised form 21 May 2006; accepted 22 May 2006
Available online 23 June 2006

Abstract

Single-walled carbon nanotubes were co-functionalized with pyrenemethanol and 3,5-dihexadecanyloxybenzyl alcohol in different ratios with the purpose of altering the content of pyrene moieties tethered to the nanotube surface. The functionalized nanotube samples were characterized by using established instrumental techniques. The absorption and emission results of the samples suggest that there are significant "intramolecular" excited-state energy transfers from both pyrene monomer and excimer to the linked nanotube, though the energy transfer efficiencies may be different between the monomer and excimer. The excimer formation can be limited by reducing the pyrenemethanol fraction to simplify the excited state processes, but contributions from the luminescence of the well-functionalized carbon nanotubes in the same wavelength region becomes an additional complication. Mechanistic implications of the photophysical results are discussed.

Keywords: Single-walled carbon nanotubes; Functionalization; Energy transfer

1. Introduction

Carbon nanotubes have been coupled with various chromophores for the exploration of opto-electronic properties of the resulting materials [1–13]. Among widely investigated chromophores are derivatized anthracene, pyrene, porphyrin, phthalocyanine, ferrocene, and some conducting polymers [1–16]. An interesting topic in the investigations has been the excited-state energy transfer from the chromophores to carbon nanotubes [1,2,5–12]. For example, carbon nanotubes have been functionalized by molecules containing pyrene derivatives [1,2,12]. In the work of Georgakilas et al., the functionalization was based on the addition of azomethine ylide to the sidewall of single-walled carbon nanotubes (SWNTs), with on average one pyrene unit per 95 nanotube carbons in the resulting sample [2]. It was found that the excited state of the pyrene moieties was significantly quenched by the attached nanotube. Sun and coworkers functionalized carbon nanotubes with tethered pyrene moieties in a different configuration [1,12]. These samples with carbon nanotube contents of 15–30% by weight were readily soluble in common organic solvents, so that their photoexcited state properties could be studied in homogeneous solution. According to the fluorescence results, there were both pyrene monomer and excimer contributions in the observed emissions, and the pyrene emissions were significantly quenched by the attached carbon nanotubes [1,12]. More quantitatively, the monomer versus excimer emission competition and the quenching of pyrene excited states by the nanotubes were both dependent on the pyrene population on the nanotube surface as well as the tether length and characteristics [1,12].

The observation of pyrene excimer emission even in the functionalized nanotube samples of low pyrene contents may reflect the fact that multiple defects on the nanotube surface are in clusters, which thus allow two or more tethered pyrene moieties to be in close proximity. In the study of excited-state energy transfer from pyrenes to the attached nanotubes, a relatively simpler mechanistic picture may emerge if the excimer formation is minimized. However, a further reduction in pyrene population on the nanotube surface is limited by the requirement for a sufficient number of functional groups to maintain the solubilization of the nanotubes. Therefore, in this work we

* Corresponding author. Tel.: +1 864 656 5026.
E-mail address: syaping@clemson.edu (Y.-P. Sun).

1010-6030/$ – see front matter © 2006 Elsevier B.V. All rights reserved.
doi:10.1016/j.jphotochem.2006.05.017

introduced co-functional groups that contain no pyrene moieties to balance the solubilization requirement. Pyrenemethanol and 3,5-dihexadecanyloxybenzyl alcohol (G_1OH) were used in different ratios to co-functionalize SWNTs in esterification reactions [17,18]. The resulting samples (**I–III**) were characterized by using microscopy and spectroscopy techniques. The fluorescence properties of these compounds as relevant to the excited state pyrene-to-nanotube energy transfer are reported and discussed.

2. Experimental section

2.1. Materials

Methyl 3,5-dihydroxybenzoate (98%) and 18-crown-6 (98%) were purchased from Avocado Research Chemical, thionyl chloride (99.5%), anhydrous potassium carbonate, and 1-bromohexadecane (99%) from Acros, 1-pyrenemethanol (98%) from Aldrich, and magnesium sulfate (99.5%) and lithium tetrahydridoaluminate (95%) from Alfa Aesar. The PVDF dialysis tubing (molecular weight cutoff ~1 million) was obtained from Sigma. All solvents were either of spectrophotometry/HPLC grade or purified via simple distillation. THF was distilled over sodium before use. Deuterated solvents for NMR measurements were supplied by Cambridge Isotope Laboratories.

SWNTs were produced by the arc-discharge method [19]. The purification was based on the classical oxidative acid treatment as already reported in the literature [20].

2.2. Measurements

NMR measurements were performed on a JEOL Eclipse +500 NMR spectrometer. Raman spectra were recorded on a Renishaw Raman spectrometer equipped with a 50 mW solid-state laser for 785 nm excitation. FT-IR spectra were measured on a Thermo-Nicolet Nexus 670 FT-IR spectrometer. Thermogravimetric analysis (TGA) was carried out on a Mettler-Toledo TGA/SDTA851 system. Transmission electron microscopy (TEM) images were obtained on a Hitachi HF-2000 TEM system equipped with a Gatan Multiscan CCD camera for digital imaging.

UV–vis absorption spectra were recorded on a Shimadzu UV2501 spectrophotometer. Fluorescence spectra were obtained on Spex Fluorolog-2 and Fluorolog-3 photon-counting emission spectrometers, both equipped with a 450-W xenon source. Unless specified otherwise, all emission spectra were corrected for nonlinear instrumental response by use of predetermined correction factors. Fluorescence decays were measured by using time-correlated single photon counting (TCSPC) method. The TCSPC setup consisted of a nitrogen flash lamp (Edinburgh Instruments), a 337 nm band-pass filter (10 nm FWHM), and a Phillips XP2254/B (red sensitive version of XP2020) PMT in a thermoelectrically cooled housing. The instrumental response function of the setup was ~2 ns (FWHM). All solutions used in fluorescence measurements were degassed in repeated freeze-pump-thaw cycles.

2.3. Co-functionalization of SWNTs

3,5-Dihexadecanyloxybenzyl alcohol (G_1OH) was synthesized as reported in the literature [17]. Briefly, methyl 3,5-dihydroxybenzoate (5.04 g, 30 mmol), 1-bromohexadecane (18.3 mL, 60 mmol), anhydrous K_2CO_3 (8.3 g, 60 mmol), and 18-crown-6 (0.396 g, 1.5 mmol) were dissolved in THF/acetonitrile (4/1, 400 mL), and the solution was refluxed for 36 h under nitrogen gas protection. The reaction mixture was filtered, followed by recrystallization to obtain methyl 3,5-dihexadecanyloxybenzoate (17 g, 92% yield). ^{1}H NMR (500 MHz, $CDCl_3$) δ 7.17 (d, J = 2.3 Hz, 2H), 6.63 (d, J = 2.3 Hz, 1H), 3.96–3.95 (t, J = 6.65 Hz, 4H), 3.90 (s, 3H), 1.80–1.74 (m, 4H), 1.47–1.43 (m, 4H), 1.26 (s, 48H), 0.91–0.86 (t, J = 6.62 Hz, 6H) ppm; ^{13}C NMR (125 MHz, $CDCl_3$) δ 167.10, 160.24, 131.87, 107.68, 106.64, 68.39, 52.27, 32.02, 29.80, 29.76, 29.69, 29.66, 29.46, 29.33, 26.14, 22.79, 14.22. The compound (3 g, 4.8 mmol) was dissolved in dry diethyl ether (350 mL), and to the solution was added $LiAlH_4$ (0.25 g, 6.25 mmol). After the solution was refluxed for 24 h under nitrogen gas atmosphere, ice water (50 g) was added. The ether phase was collected, and the aqueous phase was extracted with diethyl ether (three repeats of each 50 mL). G_1OH was obtained from the combined diethyl ether solution quantitatively. ^{1}H NMR (500 MHz, $CDCl_3$) δ 6.49 (d, J = 2.3 Hz, 2H), 6.37 (d, J = 2.3 Hz, 1H), 4.62 (d, J = 6.4 Hz, 2H), 3.93 (t, J = 6.65 Hz, 4H), 1.80–1.73 (m, 4H), 1.45–1.41 (m, 4H), 1.30 (s, 48H), 0.89–0.87 (t, J = 6.62 Hz, 6H) ppm; ^{13}C NMR (125 MHz, $CDCl_3$) δ 160.63, 143.26, 105.12, 100.61, 68.15, 65.58, 32.03, 29.80, 29.77, 29.71, 29.68, 29.49, 29.35, 26.14, 22.79, 14.22.

The co-functionalization of SWNTs with pyrenemethanol and G_1OH was achieved via the esterification of nanotube-bounded carboxylic acids (Scheme 1). For **I**, a purified nanotube sample (30 mg) was refluxed (75 °C) in thionyl chloride (5 mL) with vigorous stirring under nitrogen gas protection. Upon a complete removal of the excess thionyl chloride, pyrenemethanol (30 mg, 0.13 mmol) and G_1OH (90 mg, 0.153 mmol) were added. The mixture was vigorously stirred at 100 °C for 24 h under nitrogen gas protection, and then cooled to room temperature for dispersion into chloroform. The chloroform dispersion was dialyzed in PVDF membrane tubing (molecular weight cutoff ~1 million) against fresh chloroform for 3 days, followed by centrifugation (3000 × g) for 30 min to obtain a dark-colored homogeneous solution. After solvent removal, the compound **I** was obtained as a dark-colored solid. ^{1}H NMR (500 MHz, $CDCl_3$) δ 8.2–7.6 (broad, pyrene), 6.8–6.0 (broad, benzene rings), 4.4–3.1 (broad, methylene groups adjacent to oxygen and pyrene), 2.2–0.5 (broad, alkyl chains in G_1OH) ppm. Compounds **II** and **III** were similarly prepared, and their NMR spectra were similar to that of **I**.

3. Results and discussion

3.1. Synthesis and characterization

The nitric acid treatment in the purification of SWNTs is known to introduce carboxylic acids (up to 2–3%) at the sur-

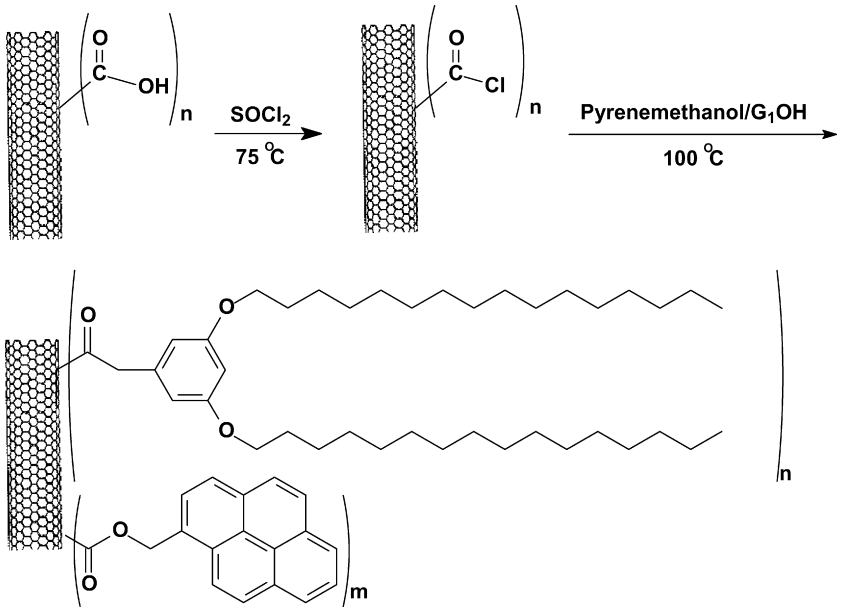

Scheme 1.

face defect sites (including broken ends) [21]. These clusters of defects, inter-spaced by sections of normal nanotube surface [22], were targeted for the covalent functionalization of carbon nanotubes. The thionyl chloride treatment converted the acids into acyl chlorides for their reaction with the various pyrenemethanol–G_1OH mixtures in 1/3, 1/9, and 1/15 weight ratios (or 1/1.2, 1/3.6, and 1/6 in molar ratios, respectively). The functionalized nanotube samples were placed in the PVDF dialysis tubing compatible with organic solvents for dialysis against fresh chloroform. With the large molecular weight cutoff (1 million) of the dialysis tubing, the removal of all lower molecular weight species other than the functionalized SWNTs was expected. The resulting pyrenemethanol–G_1OH co-functionalized nanotube samples **I–III** were generally soluble in various organic solvents, such as toluene or even hexane under ambient conditions. However, the solubility among the samples appeared to increase with the G_1OH contribution in the co-functionalization. The solubility of the samples did allow their solution-phase NMR characterization. The observed ^{1}H NMR signals for all three compounds were generally broad, but consistent with the expected functionalities in the samples. The relative signal integrations between the pyrenemethanol and G_1OH functionalities were used to estimate their actual ratios in the co-functionalized nanotube samples. The results were 1/1.5 in molar ratio for **I**, 1/5.7 for **II**, and 1/11.5 for **III**, somewhat different from the ratios of reactants used in the co-functionalization reaction. It appears that the co-functionalization and solubilization of SWNTs were in favor of more G_1OH in the final products.

The contents of SWNTs in the pyrenemethanol–G_1OH co-functionalized samples were estimated by selectively removing the functionalities in TGA analyses. The TGA scans for these samples were in a rate of 5 °C/min from 25 to 800 °C in nitrogen atmosphere. As shown in Fig. 1, the weight loss associated with the removal of pyrenemethanol and G_1OH functionalities completed at a similar temperature for all three samples. Since SWNTs are known to be stable in nitrogen atmosphere below 800 °C, the residues could be attributed to the remaining nanotubes. Thus, the estimated SWNT contents in the samples **I–III** are 42%, 20%, and 27% by weight, respectively.

These functionalized samples were also characterized by FT-IR and Raman. The FT-IR spectra of **I–III** are structurally similar. The absence of OH stretching vibration in the range of 3400–3000 cm^{-1} and the emergence of C=O mode at ~1735 cm^{-1} are consistent with the functionalization with ester linkages. Additionally, the intensity of C=C–H vibration at 3100–3000 cm^{-1} decreases in the order of **I** > **II** > **III**, indicative of the decreasing content of pyrenemethanol. The Raman spectra of **I–III** exhibit strong interference from the nanotube luminescence (due to the well-dispersion and passivation of nanotube surface defects as a result of the functionalization) [23–27]. However, after thermal defunctionalization to remove

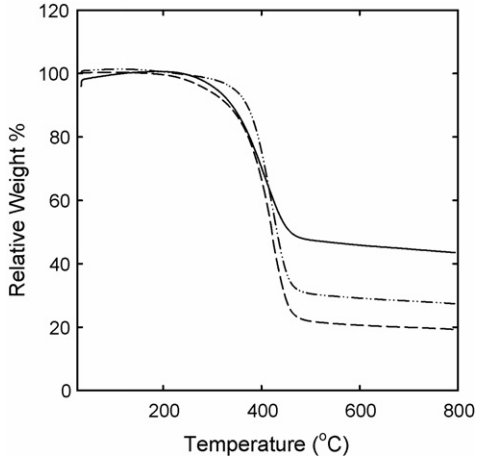

Fig. 1. TGA traces of **I** (—), **II** (– – –), and **III** (–·–) in nitrogen atmosphere (5 °C/min scan rate).

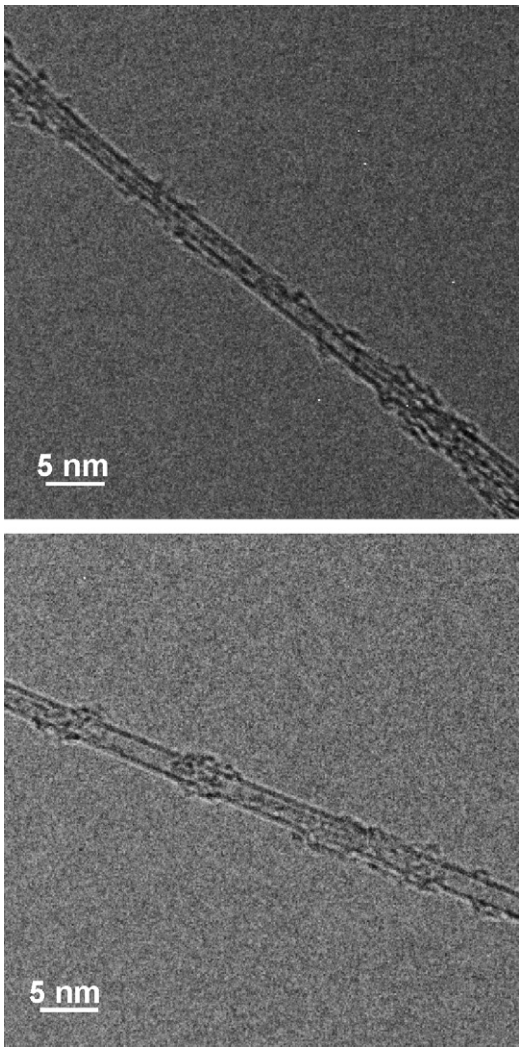

Fig. 2. High-resolution TEM images of **I** (top) and **III** (bottom) specimens.

the organic functional groups on the nanotube surface, the Raman features characteristic of SWNTs could be recovered, as expected [18,27].

The specimen for TEM analyses was prepared for each of the three samples by depositing a few drops of a dilute chloroform solution of the sample onto a holey carbon-coated copper grid, and then removing the solvent via evaporation under ambient conditions. As shown in Fig. 2, the high-resolution TEM imaging allowed the observation of individual functionalized SWNTs, where the soft materials on the nanotube surface might be attributed primarily to the organic functionalities. In a similar study reported previously, the correspondence between observed soft materials and functional groups used in the surface modification was confirmed by using high-resolution TEM coupled with electron energy loss spectroscopy (EELS) [28].

3.2. Absorption and emission

Optical absorption spectra of **I**–**III** in room-temperature methylene chloride solutions are shown in Fig. 3. The characteristic near-IR absorption bands associated with van Hove singularity transitions in semiconducting SWNTs (S_{11} and S_{22}) could still be observed with the use of a highly concentrated sample solution or thin film (Fig. 3, inset). This is consistent with the suggestion from similar investigations that the functionalization targeting nanotube surface defect sites generally preserves the band-gap electronic transitions [29,30]. However, this work concerned mostly the optical transitions in the region for pyrene, namely the solution concentrations were generally very dilute, which made the S_{11} and S_{22} absorptions negligible for most of the sample solutions.

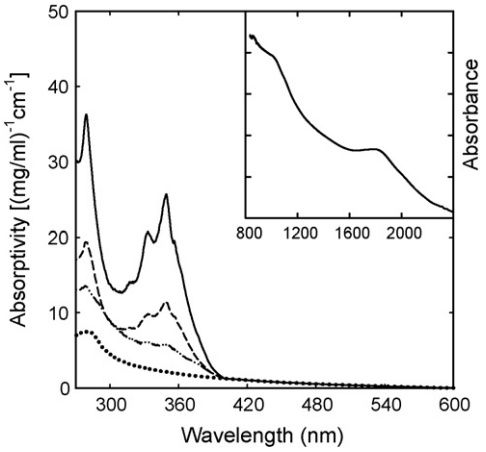

Fig. 3. UV–vis absorption spectra of **I** (—), **II** (– – –), **III** (–···–), and G_1OH-SWNT (· · ·) in room-temperature methylene chloride solutions. The inset is the absorption of **I** (concentrated solution) in the near-IR region.

The structured absorption bands of the pyrene species in these functionalized nanotube samples are apparently broadened, consistent with the previously reported findings on the absorption bands of similar compounds [1,12]. The absorption bands are also red-shifted about 5 nm from those in the spectrum of pyrenemethanol. These absorption spectral changes may be attributed primarily to effects of the heterogeneous environment associated with a distribution of different functionalization sites on the nanotube surface. The observed spectral features suggest that the contribution of pyrene absorption decreases from **I** to **III** (Fig. 3), as expected. Absorptions due to carbon nanotubes are significant in these samples. By assuming the molar absorptivity of pyrenemethanol unchanged before and after the nanotube attachment, the molar ratios between pyrenemethanol and G_1OH functionalities in the co-functionalized nanotube samples could be estimated from the absorption results: 1/1.4 for **I**, 1/5.7 for **II**, and 1/12 for **III**, in reasonable agreement with those estimated from the NMR analyses discussed above.

Fluorescence spectra of **I**–**III** in room-temperature methylene chloride solutions are shown in Fig. 4. Each spectrum (337 nm excitation) is composed of a structured band around 390 nm and a broad band centered at about 490 nm. For all three samples, the fluorescence spectra are independent of solution concentrations, suggesting the intramolecular (on the same nanotube) nature of the observed emissions. The structured band at around 390 nm is attributed to the monomer emission from derivatized pyrene

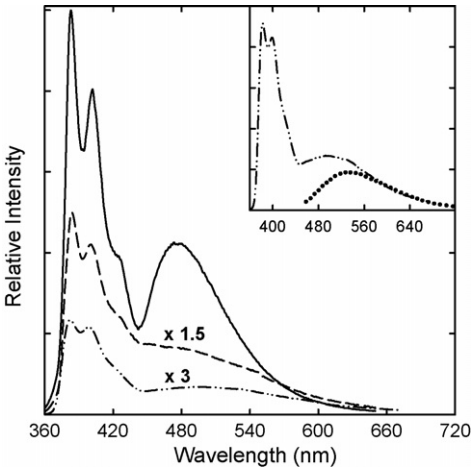

Fig. 4. Fluorescence spectra (337 nm excitation) of **I** (—), **II** (– – –), and **III** (–·–) in room-temperature methylene chloride solutions. Shown in the inset is a comparison of the spectrum of **III** with that of G_1OH-SWNT.

species tethered to the nanotube surface [1,12]. However, the broad band centered at about 490 nm is probably more complex than just the contribution of the pyrene excimer emission. From **I** to **III**, the content of pyrene moieties decreases, so that the excimer emission relative to the monomer emission should decrease significantly. Such decreases are not fully reflected in the observed spectra because the growing relative contribution from the luminescence of nanotubes themselves. It is now established that well-dispersed carbon nanotubes upon surface passivation via functionalization display visible luminescence in the same wavelength region [23–27]. This is best illustrated by the luminescence spectrum of G_1OH-functionalized SWNTs (containing no pyrene moieties at all), which obviously overlaps with the pyrene excimer emission (Fig. 4, inset).

The presence of nanotube luminescence contribution to the observed emission band at about 490 nm is reflected in the excitation spectra observed by monitoring at different emission wavelengths (Fig. 5). For **I**, the agreement between the excitation spectra monitored at 390 and 490 nm suggests dominant contribution of pyrene excimer to the emission band at about 490 nm. There is only a weak tail beyond 400 nm in the excitation spectrum monitored at 490 nm attributable to the nanotube emission. The results are as expected, because of the relatively high content of pyrene moieties in **I**. For **III** as the other extreme, the excitation spectral profiles corresponding to 390 and 490 nm emissions are different, with the spectrum monitored at 490 nm being significantly broader, consistent with a superposition of excitations for both pyrene moieties and emissive functionalized nanotubes. According to a rough decomposition of the excitation spectra by using the spectrum of G_1OH-functionalized SWNTs obtained under similar experimental conditions, the estimated contributions of nanotube emission to the observed 490 nm bands are 5% for **I**, 20% for **II**, and 40% for **III**.

Fluorescence quantum yields of **I–III** in degassed methylene chloride solutions were determined at room temperature with excitation into the pyrene absorption band (337 nm). The results including all emission contributions are 0.15 ± 0.01 for **I**, 0.13 ± 0.02 for **II**, and 0.07 ± 0.03 for **III**. Apparently, the pyrene moieties are much less fluorescent in these functionalized nanotube samples than in free pyrenemethanol (quantum yield 0.67), suggesting significant intramolecular (between the linked pyrene and nanotube) quenching of the pyrene excited states due to energy transfer to the attached nanotube [1,12]. Since the contribution of nanotube luminescence increases from **I** to **III**, the decrease in the pyrene fluorescence quantum yield from **I** to **III** is even more dramatic than what the observed overall quantum yields suggest. Therefore, an obvious conclusion is that the quenching of photoexcited pyrene moieties is more pronounced in the functionalized nanotube sample with a lower population of the methylpyrene functionality. A mechanistic explanation on the results is that the excited pyrene monomer and excimer might have different efficiencies in the energy transfer to their attached carbon nanotube. From **I** to **III**, the content of pyrene relative to G_1OH on the nanotube surface decreases, so is the excimer formation. It could be that the energy transfer to the nanotube from the excimer is less efficient than from the excited monomer, due to effects such as steric hindrance. Since the quenching of pyrene fluorescence by the attached nanotube is to a large extent static in nature [1,12], it might be easier for the pyrene monomer than the excimer to achieve a pyrene-nanotube spatial configuration required for or favorable to the energy transfer quenching.

Fluorescence decays of **I–III** in degassed methylene chloride solution were measured by exciting at 337 nm and monitoring emissions at 390 and 490 nm. As shown in Fig. 6, the decays are generally non-exponential, suggesting complicated deactivation processes of pyrene moieties in these compounds, and the decays are overall significantly faster than those of typical pyrene derivatives [31,32]. The decay curves were deconvoluted in multi-exponential fits (up to three components), and the results thus obtained are shown in Table 1. The three component lifetimes were averaged as following [33]:

$$\tau_{\text{average}} = \sum A_i \tau_i \quad (1)$$

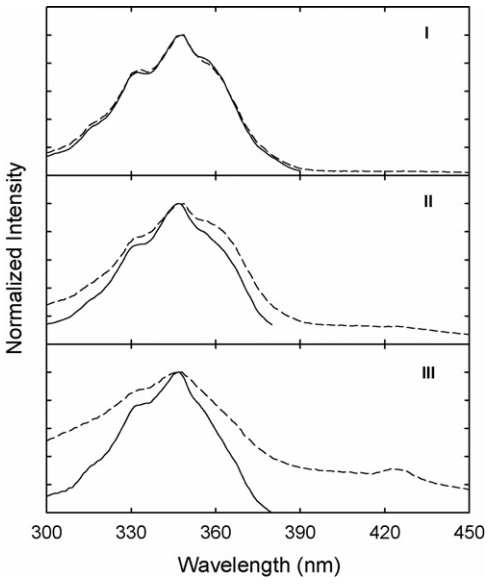

Fig. 5. Fluorescence excitation spectra of **I–III** in room-temperature methylene chloride solutions with emission monitored at 390 nm (—) and 490 nm (– – –).

Table 1
Results from fluorescence decays of **I–III** in solution (337 nm excitation)

Compound	Fluorescence decay results[a]					
	Monitored at 390 nm			Monitored at 490 nm		
	τ (ns)	A (%)	τ_{Ave} (ns)	τ (ns)	A (%)	τ_{Ave} (ns)
	7.2	6.69		3.3	4.55	57.8
I	27.4	37.9	68.5	34.8	41.5	
	104	55.4		80.1	54	
	8.2	4.07		7.3	31.5	33.8
II	31.5	30	75.1	16.9	27	
	99.1	65.9		65	41.4	
	3.2	5.01		9.2	70.1	19.4
III[b]	28.2	24.4	76.7	43.2	29.9	
	98.7	70.6				

[a] Decay curves deconvoluted with a three-exponential function.
[b] The decay monitored at 490 nm could be fitted with a two-exponential function.

where A_i and τ_i are the pre-experimental factor (in percentage) and the lifetime of the component i, respectively. The average fluorescence lifetimes calculated from Eq. (1) are also listed in Table 1.

For emissions monitored at 390 nm, the average lifetimes of **I–III** are all about 70 ns, much shorter than that of pyrenemethanol (about 300 ns in mono-exponential decay) [34], consistent with the fluorescence quenching due to the pyrene-to-nanotube energy transfer. However, the decrease in lifetime as a result of the quenching is less than that in the quantum yield, again suggesting the contribution of static quenching associated with the excited-state energy transfer, as reported and discussed previously [1,12]. For the emissions monitored at 490 nm, the average lifetime is progressively shorter from **I** to **III** (Table 1). Since the multi-exponential fit is primarily an empirical treatment, it is hardly meaningful to scrutinize the changes in different lifetime components. Instead, the shortening in the average decay lifetime for the 490 nm emissions from **I** to **III** may simply be attributed to growing contributions from the short-lived (less than 10 ns) luminescence of the functionalized carbon nanotubes [23–27].

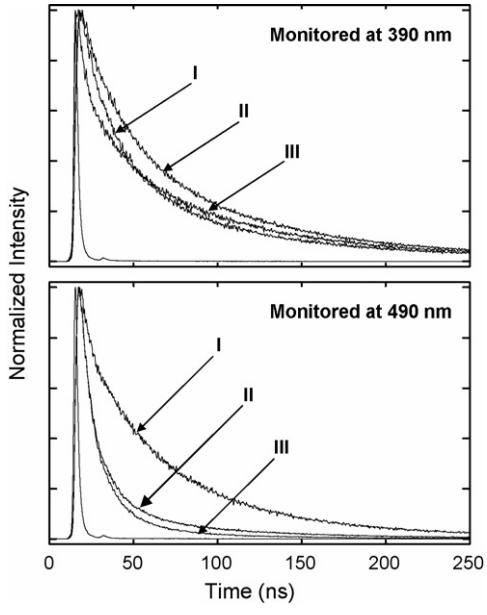

Fig. 6. Fluorescence decays of **I–III** in room-temperature methylene chloride solutions with 337 nm excitation.

The photophysical processes in these functionalized carbon nanotube samples are apparently complicated, like in many other macromolecules containing multiple pyrene species [31,32]. As stated in the introduction, the purpose of this work was to create a relatively simpler system of pyrene-containing functionalized carbon nanotubes by diluting the tethered pyrene population to the level of excimer formation becoming negligible (thus to simplify the excited state processes for a more direct probing of the pyrene-to-nanotube energy transfer). Although the intended unambiguous photophysical results are somewhat contaminated by the luminescence contribution from the functionalized carbon nanotubes, the reported results still allow an improved understanding of the excited state pyrene-to-nanotube energy transfer. However, with the confirmation on the presence of excited-state energy transfer, an interesting question is the possibility of emissions from the carbon nanotubes excited indirectly by the transferred energy. Furthermore, quantitative investigations are required in order to address this and related questions.

Acknowledgments

We thank W. Huang and K. Fu for experimental assistance. Financial support from NSF, NASA, and the Center for Advanced Engineering Fibers and Films (NSF-ERC at Clemson University) is gratefully acknowledged. Research at Oak Ridge National Laboratory was sponsored by the Assistant Secretary for Energy Efficiency and Renewable Energy, Office of FreedomCAR and Vehicle Technologies, as part of the HTML User Program, managed by UT-Battelle LLC for DOE.

References

[1] L. Qu, R.B. Martin, W. Huang, K. Fu, D. Zweifel, Y. Lin, Y.-P. Sun, C.E. Bunker, B.A. Harruff, J.A. Gord, L.F. Allard, J. Chem. Phys. 117 (2002) 8089–8094.

[2] V. Georgakilas, K. Kordatos, M. Prato, D.M. Guldi, M. Holzinger, A. Hirsch, J. Am. Chem. Soc. 124 (2002) 760–761.
[3] J. Zhang, J.-K. Lee, Y. Wu, R.W. Murray, NanoLetters 3 (2003) 403–407.
[4] G. de la Torre, W. Blau, T. Torres, Nanotechnology 14 (2003) 765–771.
[5] H. Ago, M.S.P. Shaffer, D.S. Ginger, A.H. Windle, R.H. Friend, Phys. Rev. B 61 (2000) 2286–2290.
[6] D.M. Guldi, G.M.A. Rahman, F. Zerbetto, M. Prato, Acc. Chem. Res. 38 (2005) 871.
[7] W. Zhu, N. Minami, S. Kazaoui, Y. Kim, J. Mater. Chem. 13 (2003) 2196–2201.
[8] M. Alvaro, P. Atienzar, J.L. Bourdelande, H. Garcia, Chem. Phys. Lett. 384 (2004) 119–123.
[9] N. Nakashima, Y. Tomonari, H. Murakami, Chem. Lett. (2002) 638–639.
[10] L. Liu, T. Wang, J. Li, Z.-X. Guo, L. Dai, D. Zhang, D. Zhu, Chem. Phys. Lett. 367 (2003) 747–752.
[11] D.M. Guldi, M. Marcaccio, D. Paolucci, F. Paolucci, N. Tagmatarchis, D. Tasis, E. Vázquez, M. Prato, Angew. Chem. Int. Ed. 42 (2003) 4206–4209.
[12] R.B. Martin, L. Qu, Y. Lin, B.A. Harruff, C.E. Bunker, J.A. Gord, L.F. Allard, Y.-P. Sun, J. Chem. Phys. B 108 (2004) 11447–11453.
[13] H. Li, R.B. Martin, B.A. Harruff, R.A. Carino, L.F. Allard, Y.-P. Sun, Adv. Mater. 16 (2005) 896–900.
[14] A. Star, J.F. Stoddart, D. Steuerman, M. Diehl, A. Boukai, E.W. Wong, X. Yang, S.W. Chung, H. Choi, J.R. Heath, Angew. Chem. Int. Ed. 40 (2001) 1721–1725.
[15] B. Zhao, H. Hu, A. Yu, D. Perea, R.C. Haddon, J. Am. Chem. Soc. 127 (2005) 8197–8203.
[16] G.M.A. Rahman, D.M. Guldi, R. Cagnoli, A. Mucci, L. Schenetti, L. Vaccari, M. Prato, J. Am. Chem. Soc. 127 (2005) 10051–10057.
[17] Y.-P. Sun, W. Huang, Y. Lin, K. Fu, A. Kitaygorodskiy, L.A. Riddle, Y.J. Yu, D.L. Carroll, Chem. Mater. 13 (2001) 2864–2869.
[18] Y.-P. Sun, K. Fu, Y. Lin, W. Huang, Acc. Chem. Res. 35 (2002) 1096–1104.
[19] C. Journet, W.K. Maser, P. Bernier, A. Loiseau, M.L. de la Chapelle, S. Lefrant, P. Deniard, R. Lee, J.E. Fischer, Nature 388 (1997) 756–758.
[20] J. Liu, A.G. Rinzler, H. Dai, J.H. Hafner, R.K. Bradley, P.J. Boul, A. Lu, T. Iverson, K. Shelimov, C.B. Huffman, F. Rodriguez-Macias, Y.S. Shon, T.R. Lee, D.T. Colben, R.E. Smalley, Science 280 (1998) 1253–1256.
[21] H. Hu, P. Bhowmik, B. Zhao, M.A. Hamon, M.E. Itkis, R.C. Haddon, Chem. Phys. Lett. 345 (2001) 25–28.
[22] M.A. Salazar, H. Li, Y.-P. Sun, J. McNeill, J. Nanosci. Nanotech., submitted for publication.
[23] J.E. Riggs, Z. Guo, D.L. Carroll, Y.-P. Sun, J. Am. Chem. Soc. 122 (2000) 5879–5880.
[24] Y.-P. Sun, B. Zhou, K. Henbest, K. Fu, W. Huang, Y. Lin, S. Taylor, D.L. Carroll, Chem. Phys. Lett. 351 (2002) 349–353.
[25] S. Banerjee, S.S. Wong, J. Am. Chem. Soc. 124 (2002) 8940–8948.
[26] D.M. Guldi, M. Holzinger, A. Hirsch, V. Georgakilas, M. Prato, Chem. Commun. (2003) 1130–1131.
[27] Y. Lin, B. Zhou, R.B. Martin, K.B. Henbest, B.A. Harruff, J.E. Riggs, Z. Guo, L.F. Allard, Y.-P. Sun, J. Phys. Chem. B 109 (2005) 14779–14782.
[28] Y. Lin, D.E. Hill, J. Bentley, L.F. Allard, Y.-P. Sun, J. Phys. Chem. B 107 (2003) 10453–10457.
[29] M.A. Hamon, H. Hui, P. Bhowmik, H.M.E. Itkis, R.C. Haddon, Appl. Phys. A 74 (2002) 333–338.
[30] B. Zhou, Y. Lin, H. Li, W. Huang, J.W. Connell, L.F. Allard, Y.-P. Sun, J. Phys. Chem. B 107 (2003) 13588–13592.
[31] S.E. Webber, Chem. Rev. 90 (1990) 1469–1482.
[32] K.A. Zachariasse, A.L. Macanita, W. Kuhnle, J. Phys. Chem. B 103 (1999) 9356–9365.
[33] J.R. Lakowicz, Principles of Fluorescence Spectroscopy, 2nd ed., Kluwer Academic/Plenum Publishers, New York, 1999, p. 130 (Chapter 4).
[34] G.M. Stewart, M.A. Fox, J. Am. Chem. Soc. 118 (1996) 4354–4360.